Nanoscale Res Lett (2008) 3:524–529
DOI 10.1007/s11671-008-9192-7

NANO EXPRESS

Atomistic Origin of Rate-Dependent Serrated Plastic Flow in Metallic Glasses

S. Y. Jiang · M. Q. Jiang · L. H. Dai · Y. G. Yao

Received: 7 October 2008 / Accepted: 17 October 2008 / Published online: 4 November 2008

Abstract Nanoindentation simulations on a binary metallic glass were performed under various strain rates by using molecular dynamics. The rate-dependent serrated plastic flow was clearly observed, and the spatiotemporal behavior of its underlying irreversible atomic rearrangement was probed. Our findings clearly validate that the serration is a temporally inhomogeneous characteristic of such rearrangements and not directly dependent on the resultant shear-banding spatiality. The unique spatiotemporal distribution of shear banding during nanoindentation is highlighted in terms of the potential energy landscape (PEL) theory.

Keywords Metallic glasses · Serrated plastic flow · Strain rate · Molecular dynamics

Bulk metallic glasses (BMGs), because of their long-range atomic disorder, deform uniquely [1–4]: the plastic deformation is highly localized into narrow shear bands at room temperature [5–8]. Under deformation-constrained loading modes such as compression [9–11] and nanoindentation [12–19], serrated plastic flow phenomena have been widely observed and found to be rate-dependent: as strain rate decreases, the flow serrations become more distinct. Moreover, rate-dependent shear-band patterns were observed on the surfaces or inside the post-deformed specimens under compression [10] and nanoindentation [15–17]. Therefore, currently, it is well accepted that the macroscopic serrated plastic flow behavior is associated with the shear-banding operations on a nanoscale within BMGs. Considerable efforts have been made to uncover the relationship between them. Schuh et al. [13], Schuh and Nieh [14] and Zhang et al. [18] suggested that the simultaneous operations of multiple shear bands at high strain rate result in the smooth plastic flow; with increasing strain rate, the deformation mode transits from inhomogeneous to homogeneous. However, Jiang and Atzmon [15], Greer et al. [17], and Jang et al. [19] considered that the disappearance of flow serrations at high strain rate arises from the limitation of data acquisition and the instrumental response; even at extremely high strain rate, the plastic deformation is still inhomogeneous. Since these hypotheses were mainly gained from ex situ experimental observations on shear-band patterns, the physical origin of rate-dependent serrated plastic flow, even if well accepted as a temporal event or process behavior [10, 11, 15], is still not well grounded.

Very recently, infrared camera technique has been used for in situ observing dynamic shear banding operations in the study of the serrated plastic flow during compression by Jiang et al. [10]. Based on the information from experimental observations, they conjectured a spatiotemporal picture of shear-banding during serrated flow, and further explained the inhomogeneous deformation during the indentation [10]. However, as they pointed out the propagation of a shear band is very fast; hence only mature shear bands can be captured [10], not to mention the fine shear-banding events on atomic scale. In addition, during indentation, since the shear bands develop underneath

S. Y. Jiang · M. Q. Jiang · L. H. Dai (✉)
State Key Laboratory of Nonlinear Mechanics (LNM), Institute of Mechanics, Chinese Academy of Sciences, 100080 Beijing, People's Republic of China
e-mail: lhdai@lnm.imech.ac.cn

Y. G. Yao
Beijing National Laboratory for Condensed Matter Physics, Institute of Physics, Chinese Academy of Sciences, 100080 Beijing, People's Republic of China

indenter, direct observation in situ on them is very difficult, even impossible. The molecular dynamics (MD) simulation is generally believed to be an effective way in modeling various indentation processes [20–22], providing an in situ observation on atomic motions. In this aspect, remarkable progress has been made by Falk, Langer, Shi et al. [20–23] by developing Argon's shear transformation zone (STZ) concept [2]. They found that the load-drop events in a load-displacement curve, i.e., serrated plastic flow, correspond closely to the bursts in deformation activity (irreversible atomic rearrangement) associated with shear bands [21]. Spatially, the suppression of wing-like shear bands of post-deformed specimen at higher strain rate leads to milder serrations [22]. However, how do the strain rates affect this inherent correlation between serrations and atomic rearrangements? How does the temporal behavior of such rearrangements produce the final shear-banding patterns after loading? These questions are still not well understood and deserve further investigation. In this letter, we rely on MD computer simulations to roundly probe how spatio-temporal distribution of shear-banding events on an atomic scale is related in situ to macroscopic rate-dependent serrated plastic flows in BMGs undergoing nanoindentation. Strain rate effect on this relationship and its underlying physics are discussed.

A binary amorphous alloy system, $Cu_{46}Zr_{54}$, was used in our MD simulations. In this system, atoms interact via a modified Lennard-Jones 4–8 potential of the form [24, 25]:

$$\phi(r_{ij}) = \begin{cases} -\dfrac{A}{r_{ij}^4} + \dfrac{B}{r_{ij}^8} + Cr_{ij} + D, & 0 < r_{ij} \le r_t \\ 0, & r_{ij} > r_t \end{cases} \quad (1)$$

where r_{ij} is the distance between the atoms i and j, A, B, C, and D are constants whose values are available in Ref. [25], and r_t is the truncation distance with the values of 5.08, 5.58, and 6.00 Å for Cu–Cu, Cu–Zr, and Zr–Zr pairs, respectively. The motion of each atom was evaluated by integrating the Newtonian equations of motion using velocity-Verlet method with a time step of 1 fs. To form an amorphous sample, an initial structure for the sample was built by placing all atoms into a face-centered cubic (fcc) crystal lattice in a random order, and the initial velocities of all atoms were set to be zero [26]. The initial structure was gradually heated to 2400 K for sufficiently melting, and then cooled to 1 K with the cooling rate of 25 K/ps. In this process, the NPT ensemble was used, and the pressure was kept at zero; periodic boundary conditions were used in all three directions. Then, for the subsequent indentation simulations, we set the top boundary free and fixed a layer of 6.0 Å in thickness at the bottom. Another 100 ps was carried out to a new equilibration. Finally, a three-dimensional sample (sample I) which contains 432,000 atoms with the size of 250 × 250 × 125 $Å^3$ and a two-dimensional sample (sample II) which includes 250,000 atoms with the size of 1950 × 1050 $Å^2$ were formed in this way.

A spherical indenter whose atomic nature is ignored was used in the nanoindentation simulations. The indenter was modeled by a purely repulsive potential with the form [27, 28]:

$$V(r) = E \cdot (R - r)^3 \cdot \theta(R - r) \quad (2)$$

where r is the distance from the indenter center to a sample atom, R is the radius of the indenter which is chosen as 20 Å for sample I and 400 Å for sample II, $\theta(R - r)$ is the standard step function, and E is a constant which is equal to 3.0 and 3.9 nN/$Å^2$ for a Cu atom and a Zr atom, respectively [28]. The indenter was displaced toward the top surface of the sample at a constant strain rate by keeping an invariable displacement interval of 0.1 Å and adjusting the relaxation time for each displacement interval. In this process, the control to the temperature (1 K) was only allowed in a layer of 10.0 Å in thickness which is just above the fixed layer at the bottom. For sample I, the total indentation depth was 15 Å, and three strain rates, 10^{11}, 10^{10}, and 10^9 s^{-1}, were executed; for sample II, the total indentation depth was 50 Å, and three strain rates, 4×10^{10}, 4×10^9, and 4×10^8 s^{-1}, were performed. Parallel computing was used in all the simulation processes.

The load–displacement (p–h) curves for the indentation simulations are shown in Fig. 1. Obviously, the rate-dependent serrated plastic flow phenomena can be observed: when strain rate decreases from 1a–c, flow serrations become more prominent. The result is consistent with a series of experimental observations for real metallic glasses under indentation [11–18]. It has been recognized that the serrated plastic flow, relating to shear-banding operations, occurs as a result of a number of structural rearrangements at atomic scale. The parameter $D^2_{\min}(-\Delta t, t)$, therefore, is adopted to identify such irreversible rearrangement with the form [23, 29]:

$$D^2_{\min}(t - \Delta t, t) = \sum_n \mathbf{R}_n \cdot \mathbf{R}_n^T \quad (3)$$

$$\mathbf{R}_n = [\mathbf{r}_n(t) - \mathbf{r}_0(t)] - (\mathbf{X} \cdot \mathbf{Y}^{-1}) \cdot [\mathbf{r}_n(t - \Delta t) - \mathbf{r}_0(t - \Delta t)] \quad (4)$$

$$\mathbf{X} = \sum_n [\mathbf{r}_n(t) - \mathbf{r}_0(t)][\mathbf{r}_n(t - \Delta t) - \mathbf{r}_0(t - \Delta t)] \quad (5)$$

$$\mathbf{Y} = \sum_n [\mathbf{r}_n(t - \Delta t) - \mathbf{r}_0(t - \Delta t)][\mathbf{r}_n(t - \Delta t) - \mathbf{r}_0(t - \Delta t)] \quad (6)$$

where the subscript n runs over the atoms within the interaction range of the reference atom ($n = 0$) and $\mathbf{r}_n(t)$ is

the position vector of the nth atom at time t. The parameter $D^2_{\min}(t - \Delta t, t)$ then denotes the local deviation between the true deformation denoted by $[\mathbf{r}_n(t) - \mathbf{r}_0(t)]$ and the affine deformation indicated by $(\mathrm{X}\ \mathrm{Y}^{-1})$ $[\mathbf{r}_n(t - \Delta t) - \mathbf{r}_0(t - \Delta t)]$ during the time interval $[t - \Delta t, t]$ [29]. We calculated $D_{\min}$ values of all atoms during each displacement interval (0.1 Å) to get information of in situ deformation. We selected 1.5 Å, which is about half of the average distance between a Cu atom and a Zr atom in the samples, as a cutoff of $D_{\min}$ to characterize the rearrangements that make up a plastic event at all strain rates [23, 29]. It is important to point out that the method of choosing the cutoff may be a little rough, considering its value may be affected by strain rates; nevertheless, it is efficient to judge the plastic deformation, and should not significantly change the trend. In addition, we find that choosing different cutoffs cannot change the trend of plastic flow under various strain rates. Any atom whose $D_{\min}$ value is greater than the cutoff is considered to be rearranged, and the numbers of the rearranged atoms at all intervals are displayed in Fig. 1 as histograms under p–h curves. Note that the numbers of the rearranged atoms get larger, but their distribution becomes more inhomogeneous when strain rate decreases. Moreover, when comparing the histograms with the p–h curves, a strong correlation between them was surprisingly discovered: the load-drop events (i.e., flow serrations) in the p–h curves correspond to the peak values (i.e., large numbers of the rearranged atoms) in the histograms; the more obvious the flow serration is, the larger the number of the rearranged atoms in that interval is. The phenomenon is consistent with the simulation results presented by Shi and Falk [21]. In fact, the number of the rearranged atoms can be regarded as an indication of the degree of plastic deformation in the displacement interval. Thus, we can conclude that the serrated plastic flow strongly depends on the temporal characteristic of the atomic rearrangement underpinning plastic deformation: successive low degree of plastic deformation at high strain rate leads to less pronounced serrated flow, and intermittent high degree of plastic deformation at low strain rate results in more distinct serrated flow.

To ferret out how shear bands operate during the indentation processes, we examined the spatial distributions of the rearranged atoms when flow serrations occur. As shown in Fig. 2, we found that, during a displacement interval, at high strain rate, few rearranged atoms form many small atomic clusters, and at low strain rate, many rearranged atoms form few large atomic clusters. The figure indicates that the degree of atomic rearrangement underlying flow in an individual loading step varies with strain rate or loading timescale. This kind of discrete flow event (i.e., rearranged atomic cluster) finally leads to distinguishing shear-band patterns at the maximum indenting

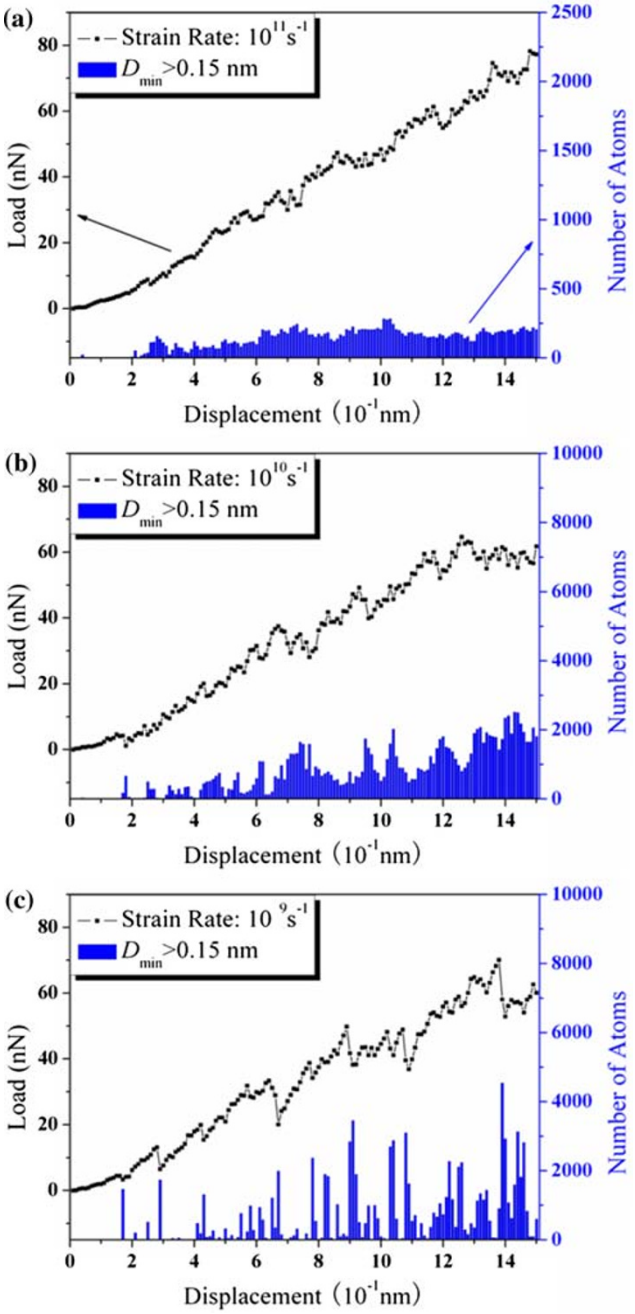

Fig. 1 The load–displacement curves and the temporal distribution of the number of rearranged atoms at various strain rates for sample I. The strain rate decreases from (**a**–**c**)

depth, which are displayed in Fig. 3: more and thinner shear bands formed at high strain rate, while fewer and coarser shear bands nucleated at low strain rate. The patterns are drawn by coloring the atoms according to their $D_{\min}(0, t)$ values; here, the darker the color the larger the $D_{\min}(0, t)$ value. They are quite similar to those observed from instrumented [15–19] and simulated [20, 22] indentations. The results in Figs. 2 and 3 were taken from sample II for the reason that larger planar size is available to display the

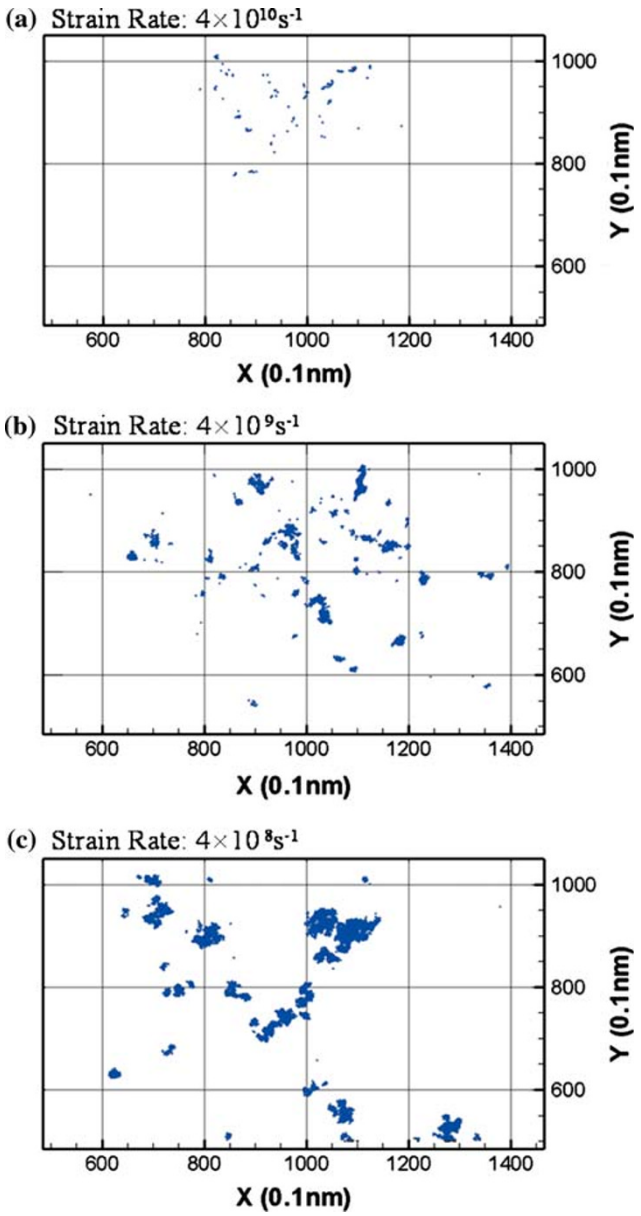

Fig. 2 The rate-dependent spatial distributions of the rearranged atoms in the displacement intervals where flow serrations occur for sample II. The strain rate decreases from (**a**–**c**); **a** strain rate 4×10^{10} s^{-1}, **b** strain rate 4×10^{9} s^{-1}, **c** strain rate 4×10^{8} s^{-1}

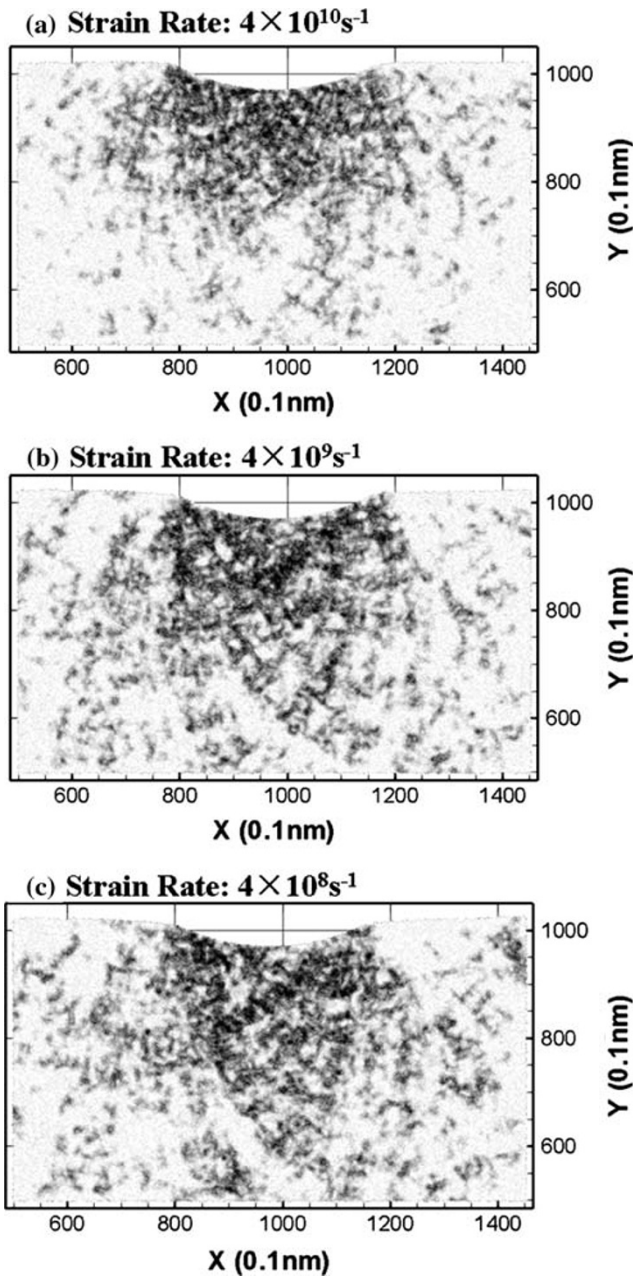

Fig. 3 The rate-dependent shear-band patterns of the maximum indenting depth for sample II. The strain rate decreases from (**a**–**c**); **a** strain rate 4×10^{10} s^{-1}, **b** strain rate 4×10^{9} s^{-1}, **c** strain rate 4×10^{8} s^{-1}

shear-band patterns. Furthermore, the potential energy versus displacement curves, as shown in Fig. 4a, were also found to be rate-dependent. With decreasing strain rate, the potential energy grows more slowly, but fluctuates more prominently; the energy-drop events essentially correspond to the load-drop events. Since our MD processes proceed at very low temperature, the potential energy which is large compared to the thermal energy must dominate the flow [30]. Thus, the unique spatiotemporal characteristic of deformation can be understood in terms of potential energy landscape (PEL) theory [30–33].

Before loading, the system stays at a local minimum of the potential energy surface (PES), and the configuration of the system is metastable. Loading will tilt the PES, and induce the disappearance of some local minima. As a result, the system will became unstable, and move to a new energy local basin. At the same time, atomic rearrangement occurs. The disappearance of a potential energy basin induced by loading is schematically shown in Fig. 4b. When transiting from one energy basin to another, the

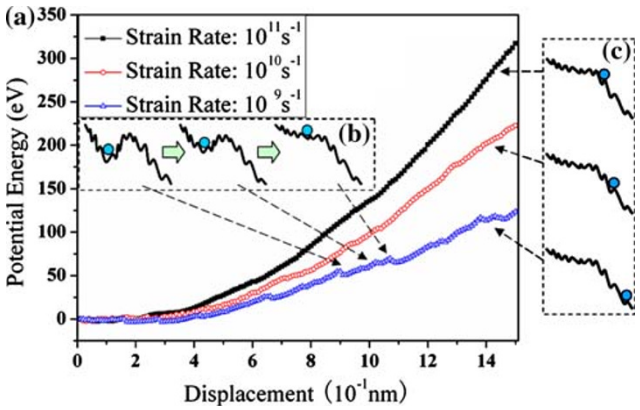

Fig. 4 (a) The potential energy versus displacement curves at different strain rates for sample I; (b) the schematic of the disappearance of a local energy minimum induced by loading; (c) the schematic of the rate-dependent systematic energy states when the system transits to a new energy basin

system at high strain rate will stay at a higher energy state in the new basin in a displacement interval than at low strain rate because of the shorter relaxation time it has. The comparison of the systematic states at different strain rates is schematically shown in Fig. 4c. Thus a whole transition of the system at high strain rate usually costs more displacement intervals, and the degree of plastic deformation at a particular displacement is relatively lower. On the contrary, at low strain rate, the system experiences less displacement intervals to reach the new basin, and the degree of plastic deformation at a particular displacement is generally higher. Hence the rate-dependent temporal distribution of deformation appears. It is this temporal characteristic of atomic rearrangement that dominates the macroscopic serrated plastic flow. On the other hand, since the potential energy of the system at the same indenting depth at high strain rate is higher, there will be more atoms at high energy state in the plastic zone. These atoms do not have enough time to rearrange. Thus, the rearrangement occurs at multiple regions, but the number of the rearranged atoms is small (see Fig. 2a). When next loading step is applied, atoms preferentially rearrange at the same positions owing to their relatively higher local energy. In other words, the shear banding preferentially operates at the same locations at higher strain rate [10]. So it is hard to conjecture from the shear-band patterns how many shear bands operate in a moment. On the other hand, the system has lower potential energy at low strain rate, so the number of the atoms with high energy state will be smaller. Thus the rearrangement happens at fewer regions. Nevertheless, the rearrangement in these few regions can develop more sufficiently, finally producing coarse shear bands (see Fig. 3c). In addition, since local atoms rearrange sufficiently, leading to a lower local energy, the atomic rearrangement at the next step must occur at other regions having high energy level. In other words, the shear bands nucleate and develop sufficiently at different positions under low strain rate. If the plastic deformation zone or spatial distribution is not related to its time, such as the uniaxial compression case [10], more and finer shear bands can finally be produced at low strain rates. However, in nanoindentation, the unique spatial patterning, fewer and coarser shear bands (see Fig. 3c), can be observed owing to space–time relationship of plastic deformation.

In summary, rate-dependent serrated plastic flow was observed in our MD simulations. The temporally inhomogeneous characteristic of the plastic deformation was revealed as the main determining factor of serrated flow behavior. It is not proper to directly relate the numbers of shear bands with the flow serrations. For example, although there is no serration in some Fe-based or Ce-based BMGs during nanoindentation, a number of fine shear bands are observed under the indents [34]. The unique rate-dependent spatiotemporal distributions of shear banding can be understood in terms of PEL theory. We believe that these findings can shed light on the relationship between microstructure and inhomogeneous plastic flow in BMGs.

Acknowledgements The work was supported by the Natural Science Foundation of China (Grants Nos. 10725211, 10721202, 10534030, 10674163), the Ministry of Science and Technology of China (2006CB921300, 2007CB925000), and the Knowledge Innovation Project & Key Project of Chinese Academy of Sciences (Nos. KJCX2-YW-M04 and KJCX-SW-L08). All computation of this work were carried out by Supercomputer DeepComp 6800, and we thank Dr. Yangde Feng of Super Computing Center of Chinese Academy of Science for his help in the computations.

References

1. F. Spaepen, Acta Met. **25**, 407 (1977). doi:10.1016/0001-6160(77)90232-2
2. A.S. Argon, Acta Metal. **27**, 47 (1979)
3. C.A. Schun, T.C. Hufnagel, U. Ramamurty, Acta Mater. **55**, 4067 (2007). doi:10.1016/j.actamat.2007.01.052
4. M.L. Falk, Science **318**, 1880 (2007). doi:10.1126/science.1150919
5. T.C. Hufnagel, P. EI-Deiry, R.P. Vinci, Scr. Mater. **43**, 1071 (2000). doi:10.1016/S1359-6462(00)00527-3
6. J. Li, F. Spaepen, T.C. Hufnagel, Philos. Mag. **82**, 2623 (2002)
7. L.F. Liu, L.H. Dai, Y.L. Bai, B.C. Wei, J. Non-Cryst. Solids **351**, 3259 (2005). doi:10.1016/j.jnoncrysol.2005.07.030
8. Y. Zhang, A.L. Greer, Appl. Phys. Lett. **89**, 071907 (2006). doi:10.1063/1.2336598
9. L.F. Liu, L.H. Dai, Y.L. Bai, B.C. Wei, J. Eckert, Mater. Chem. Phys. **93**, 174 (2005). doi:10.1016/j.matchemphys.2005.03.011
10. W.H. Jiang, G.J. Fan, F.X. Liu, G.Y. Wang, H. Choo, P.K. Liaw, Int. J. Plast. **24**, 1 (2007). doi:10.1016/j.ijplas.2007.01.015
11. W.J. Wright, R. Saha, W.D. Nix, Mater. Trans JIM **42**, 642 (2001). doi:10.2320/matertrans.42.642
12. B. Yang, T.G. Nieh, Acta Mater. **55**, 295 (2007). doi:10.1016/j.actamat.2006.08.028
13. C.A. Schuh, A.S. Argon, T.G. Nieh, J. Wadsworth, Philos. Mag. **83**, 2585 (2003). doi:10.1080/1478643031000118012

14. C.A. Schuh, T.G. Nieh, Acta Mater. **51**, 87 (2003). doi:10.1016/S1359-6454(02)00303-8
15. W.H. Jiang, M. Atzmon, J. Mater. Res. **18**, 755 (2003). doi:10.1557/JMR.2003.0103
16. L.H. Dai, L.F. Liu, M. Yan, B.C. Wei, J. Eckert, Chin. Phys. Lett. **21**, 1593 (2004). doi:10.1088/0256-307X/21/8/051
17. A.L. Greer, A. Castellero, S.V. Madge, I.T. Walker, J.R. Wilde, Mater. Sci. Eng. A **375**, 1182 (2004). doi:10.1016/j.msea.2003.10.032
18. G.P. Zhang, W. Wang, B. Zhang, J. Tan, C.S. Liu, Scr. Mater. **52**, 1147 (2005). doi:10.1016/j.scriptamat.2005.01.045
19. J.-I. Jang, B.G. Yoo, J.Y. Kim, Appl. Phys. Lett. **90**, 211906 (2007). doi:10.1063/1.2742286
20. Y. Shi, M.L. Falk, Appl. Phys. Lett. **86**, 011914 (2005). doi:10.1063/1.1844593
21. Y. Shi, M.L. Falk, Thin Solid Films **515**, 3181 (2007)
22. Y. Shi, M.L. Falk, Acta Mater. **55**, 4317 (2007). doi:10.1016/j.actamat.2007.03.029
23. M.L. Falk, J.S. Langer, Phys. Rev. E Stat. Phys. Plasmas Fluids Relat. Interdiscip. Topics **57**, 7192 (1998). doi:10.1103/PhysRevE.57.7192
24. S. Kobayashi, K. Maeda, S. Takeuchi, J. Phys. Soc. Jpn. **48**, 1147 (1980). doi:10.1143/JPSJ.48.1147
25. A.C. Lund, C.A. Schuh, Acta Mater. **51**, 5399 (2003). doi:10.1016/S1359-6454(03)00396-3
26. N.P. Bailey, Phys. Rev. B **69**, 144205 (2004). doi:10.1103/PhysRevB.69.144205
27. C.L. Kelchner, S.J. Plimpton, J.C. Hamilton, Phys. Rev. B **58**, 11085 (1998). doi:10.1103/PhysRevB.58.11085
28. X.L. Ma, W. Yang, Nanotechnology **14**, 1208 (2003). doi:10.1088/0957-4484/14/11/009
29. A. Gannepalli, S.K. Mallapragada, Nanotechnology **12**, 250 (2001). doi:10.1088/0957-4484/12/3/309
30. M. Goldstein, J. Chem. Phys. **51**, 3728 (1969). doi:10.1063/1.1672587
31. F.H. Stillinger, T.A. Weber, Science **225**, 983 (1984). doi:10.1126/science.225.4666.983
32. M.J. Osborne, D.J. Lacks, J. Phys. Chem. B **108**, 19619 (2004). doi:10.1021/jp047715z
33. S.G. Mayr, Phys. Rev. Lett. **97**, 195501 (2006). doi:10.1103/PhysRevLett.97.195501
34. W.H. Li, B.C. Wei, T.H. Zhang, D.M. Xing, L.C. Zhang, Y.R. Wang, Intermetallics **15**, 706 (2007). doi:10.1016/j.intermet.2006.10.010